SCIENTIFIC REPORTS

OPEN

High-Responsivity Multilayer $MoSe_2$ Phototransistors with Fast Response Time

Received: 28 February 2018
Accepted: 18 July 2018
Published online: 01 August 2018

Hyejoo Lee[1], Jongtae Ahn[2], Seongil Im[2], Jiyoung Kim[3] & Woong Choi[1]

There is a great interest in phototransistors based on transition metal dichalcogenides because of their interesting optoelectronic properties. However, most emphasis has been put on MoS_2 and little attention has been given to $MoSe_2$, which has higher optical absorbance. Here, we present a compelling case for multilayer $MoSe_2$ phototransistors fabricated in a bottom-gate thin-film transistor configuration on SiO_2/Si substrates. Under 650-nm-laser, our $MoSe_2$ phototransistor exhibited the best performance among $MoSe_2$ phototransistors in literature, including the highest responsivity (1.4×10^5 AW^{-1}), the highest specific detectivity (5.5×10^{13} jones), and the fastest response time (1.7 ms). We also present a qualitative model to describe the device operation based on the combination of photoconductive and photogating effects. These results demonstrate the feasibility of achieving high performance in multilayer $MoSe_2$ phototransistors, suggesting the possibility of further enhancement in the performance of $MoSe_2$ phototransistors with proper device engineering.

There is a great interest in transition metal dichalcogenides (TMDs), which are composed of vertically stacked layers held together by van der Waals interactions, because of their interesting electronic, optical, and chemical properties[1,2]. Unlike graphene, the existence of bandgaps in TMDs[3,4] such as MoS_2 or $MoSe_2$ offers an attractive possibility of using these layered materials in various device applications. Field-effect transistors (FETs) based on single or multilayer MoS_2 exhibit outstanding performance metrics, including high on/off-current ratio (~10^7), high mobility (~100 $cm^2V^{-1}s^{-1}$) and low subthreshold swing (~70 mV $decade^{-1}$)[5,6]. As the band structure of TMDs depends on their physical thickness[3,4], FETs based on TMDs are especially promising for optoelectronic devices such as phototransistors. As the optoelectronic properties of early MoS_2 phototransistors improved[7–10], high responsivity (~10^5 AW^{-1}) and fast response time (~1 ms) were obtained in MoS_2 phototransistors with device engineering such as HfO_2 encapsulation or ferroelectric gate dielectrics[11–13].

While MoS_2 has been the most extensively investigated TMD for device applications, the higher optical absorbance of $MoSe_2$[14] suggests that $MoSe_2$ could be more suitable than MoS_2 for the application of phototransistors. However, little attention has been given to the optoelectronic properties of $MoSe_2$ phototransistors, which has been less impressive than those of MoS_2 phototransistors (responsivity: 0.01–238 AW^{-1}, response time: 5–400 ms)[13,15–19]. Therefore, in this study, we explore the optoelectronic properties of $MoSe_2$ phototransistors fabricated with mechanically-exfoliated multilayer flakes on SiO_2/Si substrates. Our best-performance $MoSe_2$ phototransistor in a simple bottom-gate thin-film transistor configuration exhibits high responsivity (~1.4×10^5 AW^{-1}) and fast response time (~1.7 ms) under 650-nm-laser surpassing previously reported $MoSe_2$ phototransistors. We also investigate the dependence of photocurrent on gate voltage and optical power density to describe the device operation based on photoconductive and photogating effects. These results demonstrate the feasibility of achieving high performance in $MoSe_2$ phototransistors without complicated device structures, suggesting that the performance of $MoSe_2$ phototransistors could be further enhanced by the combination of optimized device architecture and processing.

[1]School of Materials Science & Engineering, Kookmin University, Seoul, 02707, South Korea. [2]Institute of Physics and Applied Physics, Yonsei University, Seoul, 03722, South Korea. [3]Department of Materials Science & Engineering, University of Texas at Dallas, Richardson, Texas, 75080, USA. Correspondence and requests for materials should be addressed to W.C. (email: woongchoi@kookmin.ac.kr)

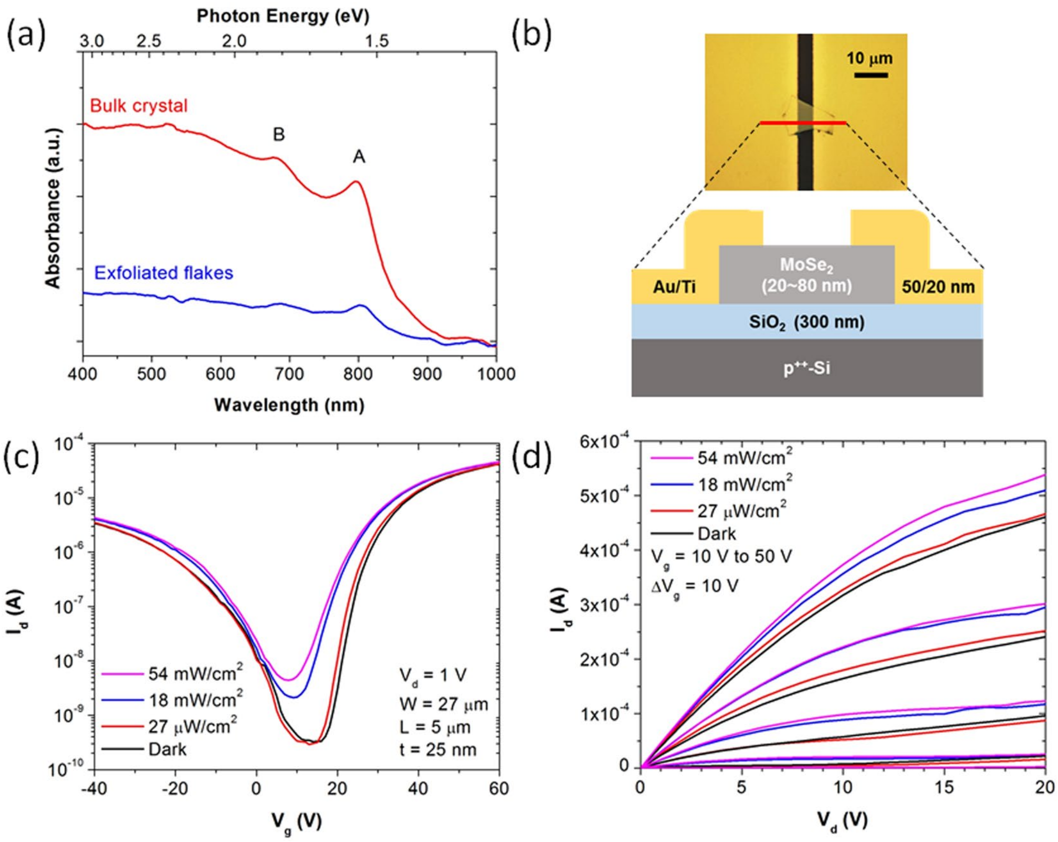

Figure 1. (**a**) Absorbance spectra of $MoSe_2$ crystals and mechanically exfoliated flakes on sapphire with two excitonic peaks A and B, (**b**) optical microscopy image and schematic cross-section of an $MoSe_2$ phototransistor along the red line, (**c**) $I_d - V_g$ and (**d**) $I_d - V_d$ characteristics of an $MoSe_2$ phototransistor with different optical power of incident light.

Results and Discussion

Before fabricating $MoSe_2$ transistors, we first measure the optical absorbance of $MoSe_2$ crystals and mechanically exfoliated flakes on sapphire substrates across visible and near-infrared spectral ranges (Fig. 1(a)). The $MoSe_2$ crystal is thicker than 100 μm and the thickness of exfoliated $MoSe_2$ flakes are in the range of 20–80 nm. Both samples show two excitonic absorbance peaks A and B at 1.55 eV and 1.82 eV, respectively, which is consistent with literature[20]. Next, multilayer $MoSe_2$ transistors are fabricated on SiO_2/Si substrates. Figure 1(b) shows the optical microscopy image of a completed $MoSe_2$ transistor along with its schematic cross-section. The measured transfer curve of an $MoSe_2$ transistor in Fig. 1(c) shows asymmetric ambipolar behavior with strong *n*-type characteristic ($MoSe_2$ thickness (t) = 25 nm). For electron transport without light, the $MoSe_2$ transistor exhibits on/off-current ratio (I_{on}/I_{off}) of 10^5 and field-effect mobility (μ_{FE}) of 50.6 $cm^2V^{-1}s^{-1}$ extracted from $\mu_{FE} = L(dI_d/dV_g)/(WC_{ox}V_d)$, where L is the channel length (5 μm), I_d is drain current, V_g is gate voltage, W is the channel width (27 μm), C_{ox} is the oxide capacitance, and V_d is the drain voltage (1 V). For hole transport without light, I_{on}/I_{off} of 10^4 and μ_{FE} of 2.8 $cm^2V^{-1}s^{-1}$ are obtained. The *n*-type-dominant ambipolar behavior of $MoSe_2$ transistors with Ti/Au electrodes was also observed in literature[21,22]. The output curves in Fig. 1(d) show linear region at low V_d suggesting decent contact properties. The transfer and output characteristics of an $MoSe_2$ transistor in Fig. 1(c,d) show the increase of I_d with the power density of incident light.

The photocurrent (I_{ph}) of phototransistors based on transition metal dichalcogenides such as $MoSe_2$ is known to be dominated by photoconductive effect and photogating effect[23]. In photoconductive effect, photogenerated excess carriers increase conductivity resulting in increased current. The photocurrent component flowing between two electrodes by photoconductive effect is given by[24] $I_{ph} = (\Delta\sigma)EWD = (\Delta n)q\mu EWD = q(\eta P_{in}/h\nu)(\mu\tau E/L)$, where $\Delta\sigma$, E, D, Δn, q, μ, η, P_{in}, h, ν, and τ are change in conductivity, electric field, depth of absorption region, change in carrier concentration, unit charge, carrier mobility, quantum efficiency, incident optical power, Planck constant, frequency of incident light, and carrier lifetime, respectively. The photoconductive component of I_{ph} is proportional to areal power density of incident light P_{in} and weakly depends on V_g[23,24]. In photogating effect, one type of photogenerated carriers (electrons or holes) is trapped in localized states and the other type of carriers flows in the channel unrecombined. As this is equivalent to doping by the other type of carriers, photogating effect accompanies a shift of threshold voltage (V_{th})[25]. As V_{th} shifts, the drain current changes from I_d to $I_d + \Delta I_d$ and it follows that[26] $I_{ph} = I_d\left(V_g - V_{th} + \Delta V_{th}\right) - I_d\left(V_g - V_{th}\right) \approx g_m\Delta V_{th} = g_m(kT/q)\ln(1 + \eta q\lambda P_{in}/I_{dark}hc)$, where g_m, k, T, λ, I_{dark}, and c are transconductance, Boltzmann constant, temperature, wavelength of incident light, dark

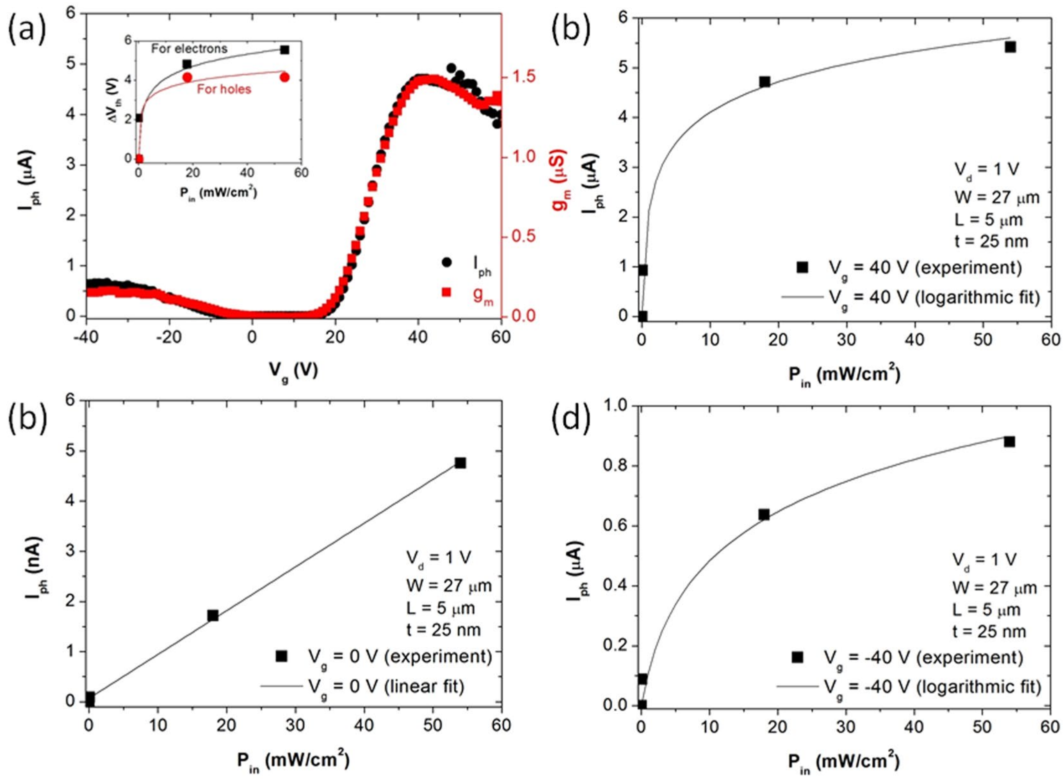

Figure 2. (**a**) I_{ph} and g_m as a function of V_g; inset shows ΔV_{th} for electrons and holes as a function of P_{in} (solid lines: logarithmic fit); I_{ph} as a function of P_{in} (**b**) at $V_g = 40$ V, (**c**) at $V_g = 0$ V, and (**d**) at $V_g = -40$ V.

current, speed of light, respectively. Thus, the photogating component of I_{ph} shows logarithmic dependence on P_{in} and is roughly proportional to transconductance (g_m)[23,26].

Figure 2(a) shows I_{ph} and g_m as a function of V_g for the same device in Fig. 1(c). The calculation of I_{ph} ($I_{ph} = I_{light} - I_{dark}$, where I_{light} is I_d in a detector with light), and g_m ($g_m = dI_d/dV_g$) is based on the data in Fig. 1(c) at $P_{in} = 18\,\mathrm{mWcm^{-2}}$. The similarity between I_{ph} and g_m suggests that photogating effect dominates the photoresponse of $MoSe_2$ transistors. In the inset of Fig. 2(a), the change in V_{th} (ΔV_{th}) for electrons and holes is shown as a function of P_{in}. The increasing change of V_{th} with increasing P_{in} also suggests the domiant role of photogating effect in our $MoSe_2$ phototransistors. However, the dependence of I_{ph} on V_g in Fig. 2(b) through (d) suggests that each effect dominates I_{ph} at different range of V_g. Figure 2(b) through (d) show I_{ph} of our $MoSe_2$ phototransistor in an on-state for electrons (at $V_g = 40$ V), an off-state (at $V_g = 0$ V), and an on-state for holes (at $V_g = -40$ V) as a function of P_{in} in sequence. I_{ph} is calculated based on the data in Fig. 1(c). The I_{ph} in an on-state for electrons (at $V_g = 40$ V) and for holes (at $V_g = -40$ V) shows logarithmic dependence on P_{in} suggesting the dominant role of photogating effect. However, the linear dependence of I_{ph} in an off-state suggests the dominant role of photoconductive effect. Such a distinct dependence of I_{ph} on V_g regime was also observed in phototransistors based on MoS_2[10], $MoTe_2$[27], compound semiconductors[26], and organic semiconductors[28].

The observed dependence of I_{ph} on V_g can be understood by the simplified energy band diagrams of an $MoSe_2$ phototransistor under a bias (V_d) at different V_g in Fig. 3. For mechanically exfoliated MoS_2 flakes and chemical vapor deposited MoS_2 films, the existence of trap state was reported in literature[13,29,30] as a result of structural defects at the surface and inside MoS_2. Similarly, we assume that electron traps and hole traps exist in the energy bandgap of $MoSe_2$ by structural defects at the surface and inside $MoSe_2$. In Fig. 3(a) (at $V_g = 40$ V), the Fermi level (E_F) is located close to the conduction band edge and the majority of electron traps are filled. Without light, I_{dark} flows by the thermionic emission or tunneling of electrons. With light, the photogenerated holes fill hole traps and additional current I_{ph} flows by the unrecombined photogenerated electrons. In Fig. 3(b) (at $V_g = 0$ V), E_F moves toward midgap and the majority of electron traps and hole traps become unfilled. Without light, I_{dark} is negligible as the high barrier height at the contact allows negligible injection of electrons and holes. With light, I_{ph} is less than that in Fig. 3(a) as the photogenerated electrons and holes recombine or fill the trap states. In Fig. 3(c) (at $V_g = -40$ V), E_F is close to the valence band edge and the majority of hole traps are filled. Without light, I_{dark} flows by the thermionic emission or tunneling of holes. With light, the photogenerated electrons fill electron traps and additional current I_{ph} flows by the unrecombined photogenerated holes.

The performance of an $MoSe_2$ transistor as a photodetector can be evaluated by responsivity (a measure of the electrical response to light) and specific detectivity (a measure of detector sensitivity)[31]. Responsivity (R) is given by $R = (I_{light} - I_{dark})/(P_{in}A)$, where A is the area of the detector. Under the assumption that shot noise from I_{dark} is the major contributor to the total noise, specific detectivity (D^*) is given by[32] $D^* = RA^{1/2}/(2qI_{dark})^{1/2}$. Figure 4(a,b) show the calculated R and D^* of the $MoSe_2$ phototransistor at different P_{in} and V_g. Maximum R of $1.4 \times 10^5\ \mathrm{AW^{-1}}$

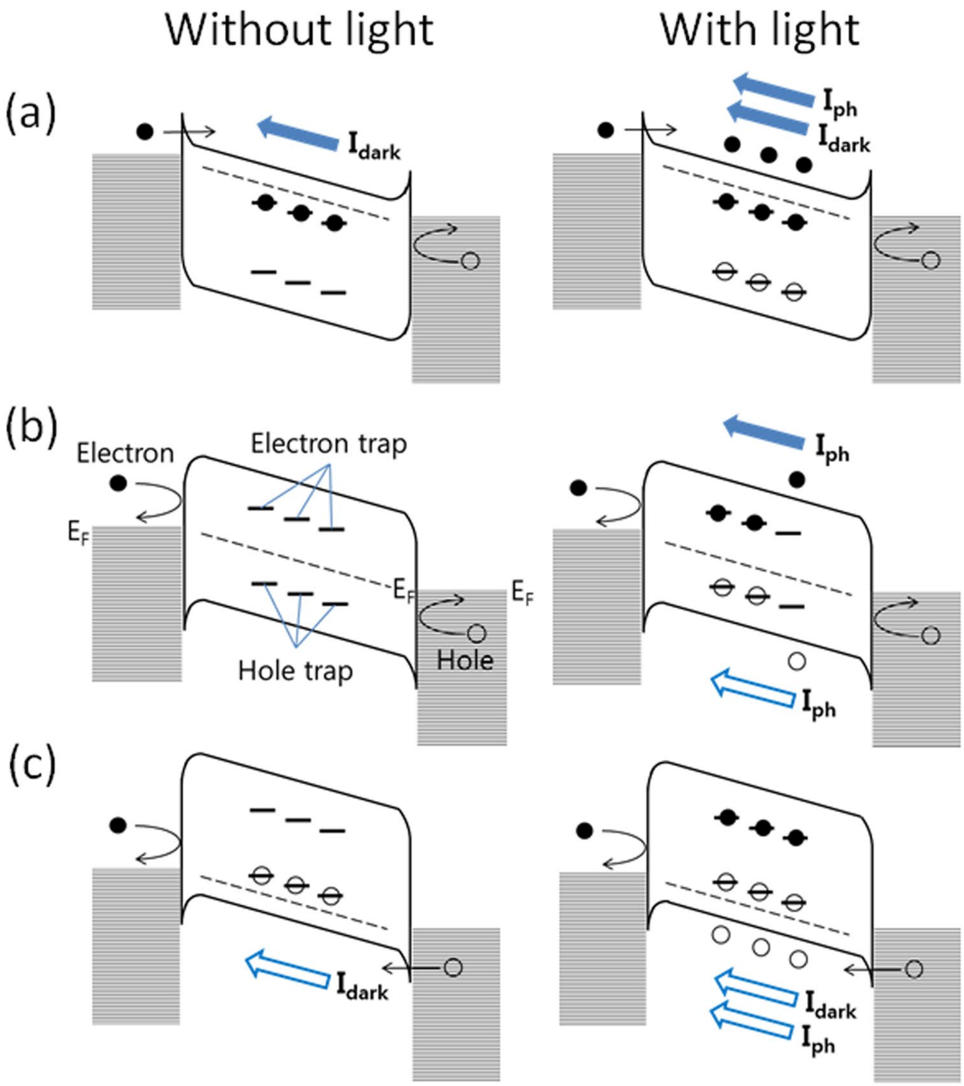

Figure 3. Schematic energy band diagrams of $MoSe_2$ phototransistors with and without light (**a**) at $V_g = 40$ V, (**b**) at $V_g = 0$ V, and (**c**) at $V_g = -40$ V under an applied bias (V_d).

and D^* of 5.5×10^{13} jones are obtained at $P_{in} = 27\,\mu\mathrm{Wcm}^{-2}$ and $V_g = 40$ V. These are the highest values of R and D^* among $MoSe_2$ phototransistors reported in literature so far ($R = 0.01$–238 AW^{-1} and $D^* = 1.0 \times 10^{11}$–7.6×10^{11} jones at $P_{in} = 10$–$100\,\mathrm{mWcm}^{-2}$)[13,15–19]. As R and D^* increase with decreasing P_{in}, the enhancement of R and D^* in this work may be due to the low P_{in} compared to that in literature. However, even at comparable P_{in} in the range of 18–54 mWcm^{-2}, the maximum R and D^* in this work ($R = 519$ AW^{-1} and $D^* = 1.3 \times 10^{12}$ jones) are about twice as high as those in literature. In Fig. 4(a,b), the overall dependence of R and D^* on P_{in} and V_g is consistent with literature[13]. R increases as P_{in} decreases or V_g increases, while D^* increases as P_{in} or V_g decreases. As P_{in} increases, more holes fill shallow trap states where lifetime is short. This results in faster recombination hence R decreases. When P_{in} increases, D^* also decreases as R decreases and I_{dark} remians unchanged. When V_g increases, electrical doping at higher V_g reduces contact resistance resulting in higher photocurrent and R. However, as V_g increases, I_{dark} also increases, which degrades D^*.

It needs to be mentioned that our $MoSe_2$ transistors show wide device-to-device variation of μ_{FE}, R, and D^* (Table S1 in Supplementary Information). Such wide device-to-device variation is commonly observed in the transistors based on transition metal dichalcogenides such as $MoSe_2$ presumably because of the variation of intrinsic defects in crystals[33]. While it is very difficult to pinpoint the origin of high performance in the best device, the correlation between R and μ_{FE} in this work (Fig. S1 in Supplementary Information) suggests that the enhanced optoelectronic properties may be related to the enhanced electrical performance of our $MoSe_2$ device. It is also supported by the fact that our $MoSe_2$ device shows the highest mobility among $MoSe_2$ transistors in Table 1.

We also note the negligible correlation between the optoelectronic properties of $MoSe_2$ devices and $MoSe_2$ thickness. This may seem counterintuitive because the width of energy bandgap changes for thin MoS_2 crystals ($< \sim 4$ nm in thickness)[4] and light absorption depends on $MoSe_2$ thickness. Yet, because the thickness of our

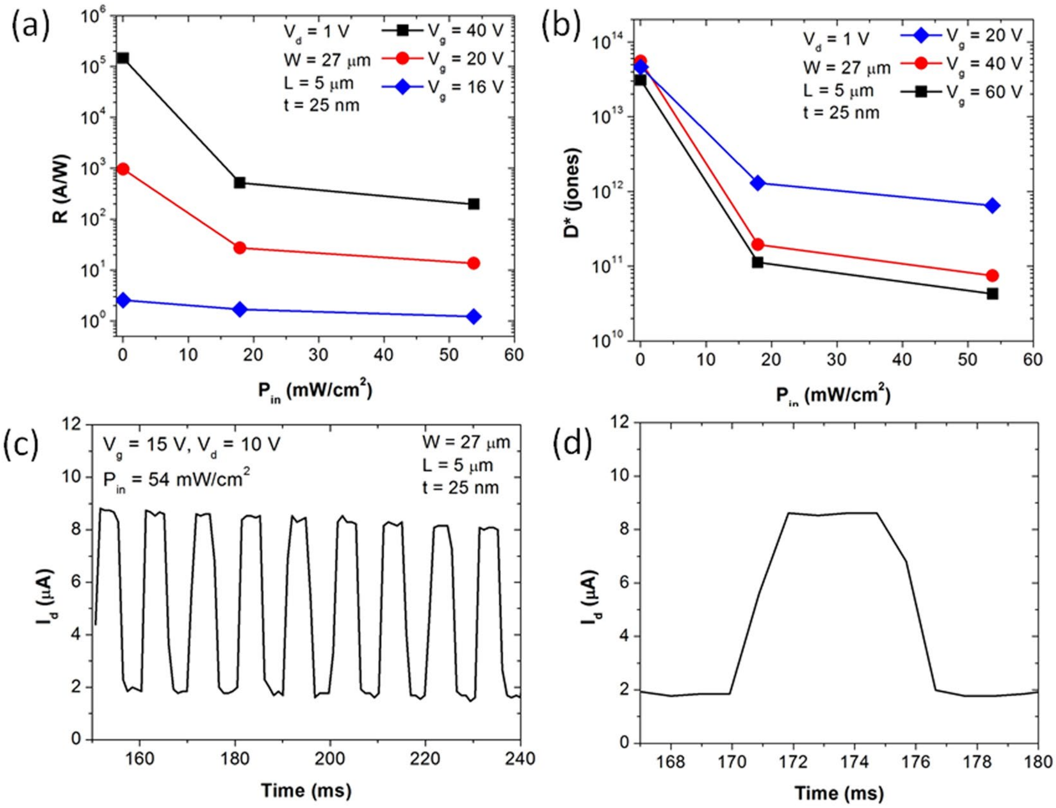

Figure 4. (**a**) R and (**b**) D^* as a function of P_{in} at different V_g; (**c**) I_d as a function of time and (**d**) zoomed-in region in (**c**).

Type of $MoSe_2$	μ_{FE} (cm^{2}v^{-1}s^{-1})	R (AW^{-1})	D^* (jones)	Response time (ms)	Reference
Multilayer flake (Exfoliation)	50.6	519.2	1.3×10^{12}	1.7 (rise) 2.2 (fall)	This work
Few layer flake (Exfoliation)	19.7	97.1	—	15 (rise) 30 (fall)	15
Single layer film (CVD)[i]	—	0.013	—	60 (rise) 60 (fall)	16
Multilayer flake (CVD)[i]	10.1	93.7	—	400 (rise) 200 (fall)	17
Multilayer flake (Exfoliation)	5.9 or 16[ii]	0.1 or 16[ii]	1.0×10^{11}[ii]	5 (fall)[ii]	13
Few layer flake (Exfoliation)	1.8	0.026	—	20 (rise) 20 (fall)	18
Few layer flake (Exfoliation)	5.1	238	7.6×10^{11}	—	19

Table 1. Performance of $MoSe_2$ phototransistors measured at $P_{in} = 10–100$ mWcm^{-2}. [i]Chemical vapor deposition. [ii]With HfO_2 encapsulation.

$MoSe_2$ flakes ranges from 20 nm to 80 nm, we expect negligible differences in energy bandgap in our $MoSe_2$ devices. On the other hand, we expect higher responsivity for devices with thicker $MoSe_2$ as more light is absorbed in thicker $MoSe_2$. However, the responsivity shows negligible correlation with thickness of $MoSe_2$ flakes in this investigation (Fig. S2 in Supplementary Information). This may be due to the variation of intrinsic materials quality overshadowing the effect of thickness. The mobility and detectivity in Fig. S2 also show negligible correlation with the thickness of $MoSe_2$ flakes, supporting this argument.

To explore the response time of our $MoSe_2$ phototransistors, we measure the time-resolved photoresponse of our $MoSe_2$ phototransistors for multiple illumination cycles. Figure 4(c) shows the result for the same device in Fig. 1(c). The incident laser with a power density of 54 mWcm^{-2} is modulated with a square wave at 100 Hz at $V_g = 15$ V and $V_d = 10$ V. The nearly identical response for multiple cycles suggests the overall rebustness and reproducibility of our $MoSe_2$ phototransistors. From a zoomed-in region in Fig. 4(d), we obtain rise time of 1.7 ms and fall time of 2.2 ms. (Rise time is calculated as the time taken by current to increase from 10% to 90% of the maximum current. Fall time is calculated as the time taken by current to decrease from 90% to 10% of the maximum current.) This is the fastest response time of $MoSe_2$ phototransistors ever reported in literature, which ranges from 5 ms to 400 ms[13,15–19]. It is intriguing that our $MoSe_2$ phototransistors exhibit high responsivity and fast response time. Because the long lifetime of carriers in photogating effect suggests slow response to light, the fast response time in our $MoSe_2$ device may be related to the characteristics of trap states. One possibility is that trap states in our $MoSe_2$ device may have shorter lifetime and higher density than those in literature. Then, while the shorter lifetime of trap states could provide fast response, the higher density of trap states could provide higher doping enhancing responsivity. However, we may only speculate at this stage and further investigation is needed on the characteristics of trap states including the distribution of trap energy, trap density, trap lifetime, and carrier capture probability.

Table 1 compares μ_{FE}, R, D^*, and response time of $MoSe_2$ phototransistors in literature. Because the measurement conditions, such as V_g, V_d, P_{in}, and excitation energy, can influence the device performance, comparable measurement conditions with those in literature are used in this work. Our $MoSe_2$ phototransistors exhibit the best performance in terms of μ_{FE}, R, D^*, and response time, demonstrating the feasibility of achieving high responsivity and fast response time in multilayer $MoSe_2$ phototransistors. Future work combining controlled growth of materials with optimized device architecture and processing will further enhance the performance of $MoSe_2$ phototransistors.

Conclusions

We report high-responsivity multilayer $MoSe_2$ phototransistors with fast response time fabricated with mechanically-exfoliated $MoSe_2$ flakes on SiO_2/Si substrates. Our $MoSe_2$ phototransistors exhibit asymmetric ambipolar behavior with strong *n*-type characteristic. Without light, high on/off-current ratio of 10^5 and field-effect mobility of 50.6 $cm^2V^{-1}s^{-1}$ are obtained for electrons. Under 650-nm-laser, our $MoSe_2$ phototransistor exhibits the best performance among $MoSe_2$ phototransistors in literature including high responsivity (1.4×10^5 AW^{-1}), high specific detectivity (5.5×10^{13} jones), fast rise time (1.7 ms) and fast fall time (2.2 ms). The dependence of photocurrent on gate voltage and optical power density suggest that photocurrent is dominated by photogating effect in on-state and by photoconductive effect in off-state. These results demonstrate the feasibility of achieving high-performance multilayer $MoSe_2$ phototransistors, providing potentially important implications on using $MoSe_2$ phototransistors for a variety of applications including touch sensor panels, image sensors, solar cells, and communication devices.

Methods

Device fabrication. Multilayer $MoSe_2$ flakes were obtained by gold-mediated mechanical exfoliation[34] from bulk $MoSe_2$ crystals (2D Semiconductors) and transferred to highly doped p-type Si wafer with thermally grown SiO_2 (300 nm). The thickness of $MoSe_2$ flakes measured by atomic force microscope (AFM, Park Systems XE-100) existed between 20 nm and 80 nm. To form source and drain electrodes (100 μm × 100 μm) on top of $MoSe_2$ flakes, Ti (20 nm) and Au (50 nm) deposited by electron-beam evaporation were patterned using photolithography and etching. The device was then annealed at 200 °C in a vacuum tube furnace for 2 hours (100 sccm Ar and 10 sccm H_2) to remove resist residue and to decrease contact resistance.

Device characterization. Optical absorbance of $MoSe_2$ was measured by UV-visible spectroscopy (Perkin-Elmer Lambda 35). Electrical characterizations were carried out with current-voltage (*I-V*) measurements (Agilent 4155 C Semiconductor Parameter Analyzer) at room temperature. The photoresponse of $MoSe_2$ phototransistors was measured with a 650-nm-laser (beam size of 3 mm) at different power densities (0.027, 18 and 54 mW cm^{-2}). Dynamic on/off switching was conducted using a function generator (Tekronix AFG310).

References

1. Wang, Q. H. *et al*. Electronics and optoelectronics of two-dimensional transition metal dichalcogenides. *Nat. Nanotechnol.* **7**, 699–712 (2012).
2. Chhowalla, M. *et al*. The chemistry of two-dimensional layered transition metal dichalcogenide nanosheets. *Nat. Chem.* **5**, 263–275 (2013).
3. Splendiani, A. *et al*. Emerging Photoluminescence in Monolayer MoS_2. *Nano Lett.* **10**, 1271–1275 (2010).
4. Mak, K. F. *et al*. Atomically Thin MoS_2: A New Direct-Gap Semiconductor. *Phys. Rev. Lett.* **105**, 136805 (2010).
5. Radisavljevic, B. *et al*. Single-layer MoS_2 transistors. *Nat. Nanotechnol.* **6**, 147–150 (2011).
6. Kim, S. *et al*. High-mobility and low-power thin-film transistors based on multilayer MoS_2 crystals. *Nat. Commun.* **3**, 1011 (2012).
7. Yin, Z. *et al*. Single-Layer MoS_2 Phototransistors. *ACS Nano* **6**, 74–80 (2012).
8. Choi, W. *et al*. High-Detectivity Multilayer MoS_2 Phototransistors with Spectral Response from Ultraviolet to Infrared. *Adv. Mater.* **24**, 5832–5836 (2012).
9. Lopez-Sanchez, O. Ultrasensitive photodetectors based on monolayer MoS_2. *Nat. Nanotech.* **8**, 497–501 (2013).
10. Zhang, W. *et al*. High-Gain Phototransistors Based on a CVD MoS_2 Monolayer. *Adv. Mater.* **25**, 3456–3461 (2013).
11. Kufer, D. *et al*. Hybrid 2D–0D MoS_2–PbS Quantum Dot Photodetectors. *Adv. Mater.* **27**, 176–180 (2015).
12. Wang, X. *et al*. Ultrasensitive and Broadband MoS_2 Photodetector Driven by Ferroelectrics. *Adv. Mater.* **27**, 6575–6581 (2015).
13. Kufer, D. & Konstantatos, G. Highly Sensitive, Encapsulated MoS_2 Photodetector with Gate Controllable Gain and Speed. *Nano Lett.* **15**, 7307–7313 (2015).
14. Bernardi, M. *et al*. Extraordinary Sunlight Absorption and One Nanometer Thick Photovoltaics Using Two-Dimensional Monolayer Materials. *Nano Lett.* **13**, 3664–3670 (2013).
15. Abderrahmane, A. *et al*. High photosensitivity few-layered $MoSe_2$ back-gated field-effect phototransistors. *Nanotechnology* **25**, 365202 (2014).
16. Xia, J. *et al*. CVD synthesis of large-area, highly crystalline $MoSe_2$ atomic layers on diverse substrates and application to photodetectors. *Nanoscale* **6**, 8949–8955 (2014).
17. Jung, C. *et al*. Highly Crystalline CVD-grown Multilayer $MoSe_2$ Thin Film Transistor for Fast Photodetector. *Sci. Rep.* **5**, 15313 (2015).
18. Hang, Y. *et al*. Photo-Electrical Properties of Trilayer $MoSe_2$ Nanoflakes. *Nano* **11**, 1650082 (2016).
19. Ko, P. J. *et al*. High-performance near-infrared photodetector based on nano-layered $MoSe_2$. *Semicond. Sci. Technol.* **32**, 065015 (2017).
20. Li, Y. *et al*. Measurement of the optical dielectric function of monolayer transition-metal dichalcogenides: MoS_2, $MoSe_2$, WS_2, and WSe_2. *Phys. Rev. B* **90**, 205422 (2014).
21. Chamlagain, B. *et al*. Mobility Improvement and Temperature Dependence in $MoSe_2$ Field-Effect Transistors on Parylene-C Substrate. *ACS Nano* **8**, 5079–5088 (2014).

22. Pradhan, N. R. Ambipolar Molybdenum Diselenide Field-Effect Transistors: Field-Effect and Hall Mobilities. *ACS Nano* **8**, 7923–7929 (2014).
23. Furchi, M. M. *et al.* Mechanisms of Photoconductivity in Atomically Thin MoS_2. *Nano Lett.* **14**, 6165–6170 (2014).
24. Sze, S. M. & Ng, K. K. *Physics of Semiconductor Devices*. 3rd ed. (Wiley, New York, 2007).
25. Buscema, M. *et al.* Photocurrent generation with two-dimensional van der Waals semiconductors. *Chem. Soc. Rev.* **44**, 3691–3718 (2015).
26. Takanashi, Y. *et al.* Characteristics of InAlAs/InGaAs high-electron-mobility-transistors under 1.3 μm laser illumination. *IEEE Electron Device Lett.* **19**, 472–474 (1998).
27. Yin, L. *et al.* Ultrahigh sensitive $MoTe_2$ phototransistors driven by carrier tunneling. *Appl. Phys. Lett.* **108**, 043503 (2016).
28. Saragi, T. P. I. *et al.* Photovoltaic and photoconductivity effect in thin-film phototransistors based on a heterocyclic spiro-type molecule. *J. Appl. Phys.* **102**, 046104 (2007).
29. Ghatak, S. & Ghosh, A. Observation of trap-assisted space charge limited conductivity in short channel MoS_2 transistor. *Appl. Phys. Lett.* **103**, 122103 (2013).
30. Zhu, W. *et al.* Electronic transport and device prospects of monolayer molybdenum disulphide grown by chemical vapour deposition. *Nat. Commun.* **5**, 3087 (2014).
31. Konstantatos, G. & Sargent, E. H. Nanostructured materials for photon detection. *Nat. Nanotechnol.* **5**, 391–400 (2010).
32. Jha, A. R. *Infrared Technology*. (Wiley, New York, 2000).
33. Schmidt, H. *et al.* Electronic transport properties of transition metal dichalcogenide field-effect devices: surface and interface effects. *Chem. Soc. Rev.* **44**, 7715–7736 (2015).
34. Desai, S. B. *et al.* Gold-Mediated Exfoliation of Ultralarge Optoelectronically-Perfect Monolayers. *Adv. Mater.* **28**, 4053–4058 (2016).

Acknowledgements

This work was supported by the National Research Foundation of Korea (Grant NRF-2013K1A4A3055679 and NRF-2016R1A2B4014369) and Industrial Strategic Technology Development Program (Grant 10045145).

Author Contributions

H.L. and W.C. designed the experiments. H.L. fabricated the devices. H.L., J.A., S.I. and J.K. characterized the devices. H.L. and W.C. wrote the manuscript. All authors reviewed the manuscript.

Additional Information

Supplementary information accompanies this paper at https://doi.org/10.1038/s41598-018-29942-1.

Competing Interests: The authors declare no competing interests.